SERS Substrates Fabricated by Island Lithography: The Silver/Pyridine System

Mino Green* and Feng Ming Liu

Imperial College London, Department of Electrical and Electronic Engineering, Exhibition Road, London, SW7 2BT, United Kingdom

Received: June 17, 2003; In Final Form: September 3, 2003

A range of pseudo-random silver structures, where there is a choice of clustered spheres or pillars or tori, have been fabricated on silicon using the method of island lithography combined with electroless plating. Pyridine has been adsorbed on these structures and the surface-enhanced Raman scattering spectrum (SERS) measured using 633 nm laser radiation. Measurements of SERS spectra as a function of pyridine solution concentration have enabled an adsorption isotherm to be obtained and the standard free energy of adsorption to be determined (24 kJ mol^{-1}), in good agreement with the literature. The substrates are found to give a uniform signal, as sampled over the prepared area, for both saturation coverage (±12%) and for a fraction of a monolayer, ca. 0.08, (±31%). It is concluded that, in the system studied, the effective area of the SERS "site" must be large compared with the area occupied by the adsorbed pyridine, so that the SERS signal is proportional to the surface coverage, averaged over the adsorbent. The formalism due to Tian and co-workers has been adopted to determine *G*, the SERS enhancement factor. *G* is calculated as follows: $G =$ (scattering intensity per adsorbed molecule)/(scattering intensity per solution molecule). *G* from 1.9×10^6 (pillars) to 2.5×10^7 (tori) have been estimated, and larger values are expected. These silver substrates, which are robust and reproducible, would seem to be good candidates for various analytical applications.

Introduction

We are here concerned to fabricate silver-containing structures, reproducibly, for Surface-Enhanced Raman Scattering (SERS) spectroscopy use in analytical chemistry. They must therefore be suitably sensitive and uniform in signal over the surface. The choice of silver as a substrate is dictated by the fact that it has the highest sensitivity for adsorbate detection; this matter and the basic science of SERS is discussed in various reviews.[1−4] The pioneering SERS work[5] was done on electrodes of electrochemically roughened silver surfaces (oxidation/reduction cycling); since then substrates of a variety of shapes have been studied.[6−8] Among the more recent structural studies, metal colloids (mostly deposited on a microscope slide) have been favored and have shown extremely large Raman signals[7] for dye molecules, especially rhodamine 6G (R6G). We question the potential stability and reproducibility (though clearly not the sensitivity) of such substrates (at least not without further improvement) and have therefore adopted a different approach, namely, the fabrication of discrete silver structures, in random array, on a silicon substrate. It is intended to test these structured substrates (where we have the choice of clustered spheres, or pillars or torus structures) in the first instance, by measuring the SERS of the simple, nonresonant, probe molecule pyridine adsorbed on the silver. This is the first phase in a program to develop a SERS-based technique for tag-free DNA analysis.

Experimental Section

Procedures. Island lithography,[9−11] involving the self-organization of a cesium chloride (CsCl) thin film into a disordered array of hemispherical islands, has been adopted for this work rather than e-beam or other beam writing procedures. This method yields high substrate densities of silver features, is suited to large area fabrication, and is within the capabilities of many well found laboratories. It seems likely from what follows that the resulting structures are well suited to SERS. The function of the CsCl hemispheres is not in this case as a resist, but rather as a lift-off material. This is so that wells can be made in a SiO_2 layer grown on Si, the wells being subsequently filled, or partly filled, with silver, and the oxide then removed if desired. The sequence of fabrication steps is shown in Figure 1. This method of fabricating silver structures is much more complicated than producing CsCl islands on top of a silver layer and then making pillars of silver by reactively ion etching (RIE) the unprotected metal. But the reason we are driven to this comparatively elaborate procedure lies in the chemistry of silver: it has no compounds that are volatile at room temperature and that are compatible with plasma etching processes.

A critical step in the fabrication sequence is the deposition of silver. Here we have adopted an electroless method that involves electrochemical displacement rather than the usual use of a reducing agent and catalyst. The method was reported by Kortenaar et al.,[12] and has been somewhat elaborated here. The over-all reaction is as follows:

$$Si(s) + 6F^-(aq) + 4Ag^+(aq) = 4Ag(s) + SiF_6^{2-}(aq)$$

It involves the reduction of silver ions, the oxidation of silicon, a dependence (but see later) on the type of charge carriers in the semiconductor, and a dependence upon the solution concentration of HF. This deposition gives rise to a range of structures.

Finally, of course, there are the spectroscopic studies on the silver substrates; for our initial tests we have chosen pyridine as the adsorbate. This is a small molecule that is not very

* Corresponding author. E-mail: m.green@imperial.ac.uk.

10.1021/jp030751y CCC: $25.00 © 2003 American Chemical Society
Published on Web 10/31/2003

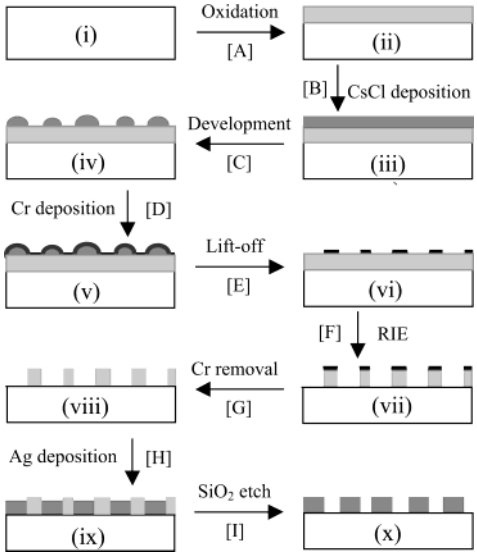

Figure 1. Process sequence for the fabrication of silver structures on a silicon base.

strongly bound to silver and has a simple Raman spectrum; it therefore represents one end of the scale of likely adsorbate/adsorbent interactions. The other end of the scale is probably typified by an adsorbate such as the dye R6G. We have also examined this latter species and will report on it in a following communication, where the subject of single molecule sensitivity arises.

Substrate Preparation. The fabrication sequence is shown in Figure 1. Step **A** (i) to (ii) depicts oxide film formation on the silicon substrate. The starting point, (i), is a p-type silicon wafer ({100} crystal orientation, resistivity 3−6 ohm cm). The silicon was placed inside a furnace: oxygen at atmospheric pressure was passed over the sample at 500 sccm and the temperature was raised to 1100 °C in 1 h, held at this temperature for 3.5 h, then allowed to cool to room temperature (∼3.5 h). This procedure gave an oxide layer that was blue and 310 nm thick, as determined using an ellipsometer (Autolit3, Rudolph Research Inc., USA). The wafer was scribed into rectangular samples 20 mm × 50 mm, and these were cleaned using a solution consisting of 1:1:1, H_2O_2 (27.5 wt %)/NH_4OH (0.88)/water. Etching was carried out for 10 min at 86 °C, after which the samples were flooded with deionized water and blow dried with dry filtered air (a procedure used after all solution treatments described below): samples at stage (ii).

The oxidized samples, freshly cleaned, yielded hydrophilic surfaces as shown by measurement of the contact angle (< 2°) of the water/SiO_2 interface.[10] Only freshly cleaned samples may be used, since several days is long enough to pick up contamination from the laboratory air leading toward a hydrophobic surface condition. The samples were then placed in a chamber evacuated by a turbomolecular pump to $< 10^{-6}$ mmHg, and CsCl, of known film thickness (L) deposited by evaporation:[10] step **B**, stage (iii). The samples were withdrawn from the vacuum chamber into a dry atmosphere (relative humidity <3%) and transferred to a development chamber. This chamber was kept at a selected and measured relative humidity (RH) by a brisk flow of moisture-controlled air: step **C**, stage (iii) to (iv). Typically, the relative humidity of the air was 40%, the CsCl film thickness, L, was 10 nm, and the development time was 60 min; which resulted in a typical array where the mean hemisphere diameter, $\langle d \rangle$, was 160 nm at a fractional area coverage, *F*, of 0.18. This follows the relation $F\langle d \rangle \approx 3L$, which is true[13] for a normal distribution of island diameters, as found here. The CsCl array of hemispheres that developed from the thin film became the template on which the lift-off process was carried out.

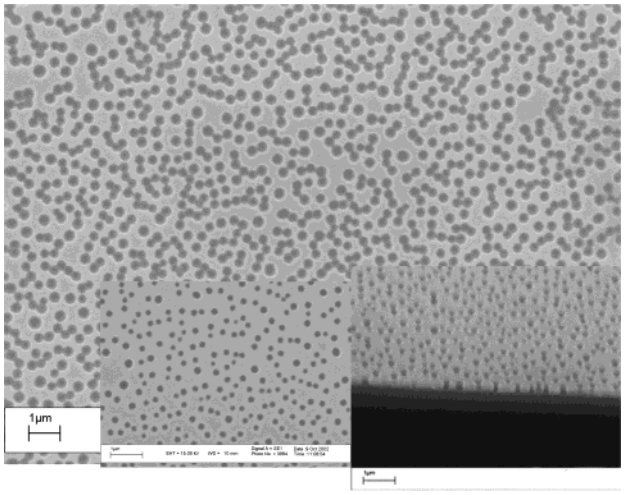

Figure 2. Perforated SiO_2 film (thickness 310 nm) on Si with Cr resist layer removed: Both insets are as made in the RIE. The inset picture shown with a 40° tilt is a broken edge showing the vertical well walls. The main picture shows the film after etching in 5% HF for 3 min. For the inset $\langle d \rangle = 0.173 \pm 0.028$ μm: $F = 0.14$. For the HF etched plate, $\langle d \rangle = 0.308 \pm 0.036$: $F = 0.365$. The size bar is 1 μm.

The lift-off process starts with the thermal deposition of a thin layer (20 nm) of chromium over the entire surface: step **D**, stage (v). Chromium or aluminum, or indeed many metals resistant to the RIE process, will do for the lift-off provided it adheres well to the SiO_2 surface and breaks away easily in the lift-off stage. We have found that 20 nm of Cr (a brittle metal) fulfils the necessary requirements particularly well. Lift-off is accomplished, step **E**, by agitation in an ultrasonic bath for 10 min, with the sample held in water in a 250 mL beaker. However, it is the case that the smallest CsCl hemispheres are not always removed and the result is that $\langle d \rangle$ is larger and *F* is smaller than the original mask set.

The sample, (iv), was transferred to the RIE apparatus (Plasmalab 80 Plus, Oxford Instruments, UK) where the exposed SiO_2 is etched away, the process stopping at the Si surface. The process parameters used were as follows: typical size, 20 mm × 30 mm; CHF_3 flow rate, 30 sccm; Ar flow rate, 20 sccm; total gas pressure, 50 mTorr; R. F. power, 180 W; and dc bias varied from 450 to 320 V. Typical etch time was 25 min; the wall angle was ca. 90°, cf. Figure 2. The chromium resist film was then stripped off using a commercial Chrome Etchant (Rockwood Electronic Materials, UK). The selectivity of the etching toward silicon is excellent. Thus inspection of the Si surface after the perforated oxide has been removed (at a broken edge) does not show surface indentation where the wells were, which would be the case if there was any etching of the Si during RIE. On the other hand, as expected, there is indentation of the Si surface at the bottom of the wells after silver deposition. All the SEM pictures in this work were taken using a No. 1450VP microscope (LEO Electron Microscope Ltd, UK).

Silver deposition, using what is here termed solution A (see below), occurs at the bottom of the wells that have been made in the SiO_2, starting at the Si/SiO_2 boundary. The sample as it comes from the RIE process, and after the Cr stripping, is prepared for deposition by washing in 1% aqueous HF solution. This treatment removes residual oxide from the Si at the well bottom and increases the well diameter. The SiO_2 (sidewall) etches at ∼23 nm/min, while the silicon at the well bottom does

TABLE 1: Silver Structures in Wells from Various Deposition Conditions[a]

no.	well treatment % HF: time, min	soln. A % HF: time, seconds	Ag structure	text figs.
(1)	1% HF: 1 min ($\langle d \rangle \sim 200$ nm)	0.12%: 120	pillars	3A
(2)	1% HF: 1 min ($\langle d \rangle \sim 200$ nm)	0.25%: 120	pillars, and a small fraction of multiple nuclei	3B
(3)	No treatment ($\langle d \rangle \sim 173$ nm)	0.25%: 120	pillars	3C
(4)	No treatment ($\langle d \rangle \sim 173$ nm)	0.5%: 20,40,60	1 to 3 nuclei, occasional torus, growing to pillar	
(5)	5%HF 3min ($\langle d \rangle \sim 308$ nm)	0.5%: 20	tori	4
(6)	1% HF: 1 min ($\langle d \rangle \sim 200$ nm)	0.5%: 120	mostly triple nuclei	
(7)	1% HF: 1 min ($\langle d \rangle \sim 200$ nm)	0.75%: 120	triple and multiple nuclei, some tori; lumps on surface	

[a] CsCl mask made from 10 nm layer, 1 h, at 40% RH: resulting well structure of $\langle d \rangle = 173$ nm, $F = 0.14$, cf. Figure 2.

not etch to any observable extent. As can be seen from Figure 2, the well diameters have a smaller percentage standard deviation after etching than the original perforated oxide, and there is some overlap of wells. Silver deposition was obtained by immersing the sample (typically 1 cm^2) in 40 mL of aqueous solution of w/w% HF and 6×10^{-3} M $AgNO_3$: (the various concentrations of HF solution in water are expressed as weight percent of HF in water). $AgNO_3$ was obtained from Aldrich, 99+% A.C.S. reagent. In using solution A, the HF concentration and immersion time were experimental variables (cf. Table 1). Flooding the system with a large excess of water terminates exposure to the silver deposition solution.

It is sometimes desired to remove the SiO_2 after the silver structures have been made. This is done using a 1:7, HF/NH_4F-buffered etchant (Rockwood Electronic Materials, UK). The etch rate is ~50 nm/min.

SERS Spectroscopy. The Raman spectra reported here were taken using a confocal Raman microscope (Renishaw 2000) with a 20× objective, of focal length 35 mm, and N.A. 0.35. The exciting radiation used through out this particular work was the 633 nm line of a He−Ne laser. The beam spot power was 2.1 mW, and the FWMH of the intensity of the (Gaussian) beam was 3.8 μm. The data were recorded without polarization analysis, and sampling times were 1−3 s, depending upon the sample.

Samples for Raman spectroscopy, typically 5 mm × 5 mm, were first placed in 40 mL of pyridine/NaCl solution of selected molarity for 30 min, the solution having been made by dilution from an aqueous solution of 0.01 M pyridine in 0.1 M NaCl. The sample was then immediately placed on the microscope stage and the spectra recorded: the samples remained observably wet throughout spectral measurement.

If the intensity of the ν_1 Raman line for pyridine in solution is compared with that obtained from the adsorbed state and suitable geometric corrections are made, a measure of the SERS enhancement factor, G, can be obtained. We have therefore measured the Raman spectrum of a 0.01 M pyridine solution in the same setup as described above. Furthermore, as discussed below, to obtain the excitation volume in this confocal setup we have adopted the following procedure. We measured the integrated Raman intensity from silicon (520.6 cm^{-1} band) as a function of the position of the plane of the silicon wafer. A depth profile, i.e., a curve of intensity versus plane position was obtained, the FWHM was taken to correspond to h, the length of the excitation volume (any correction for the absorption depth in Si can be ignored since the extinction coefficient is 0.019 at 633 nm).

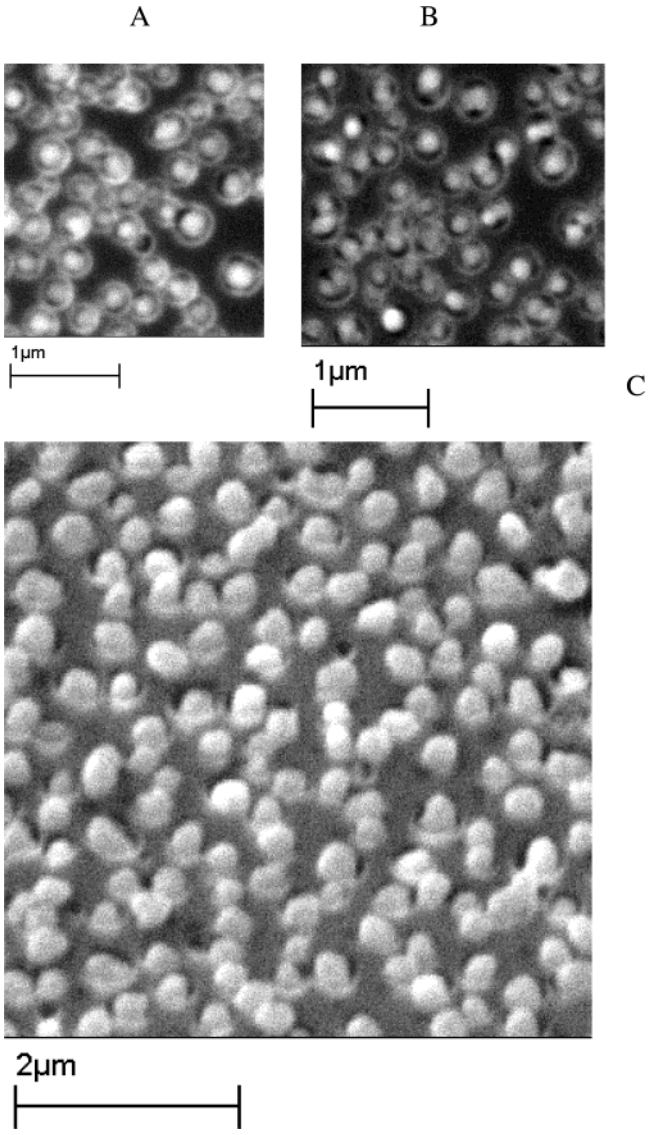

Figure 3. Effect of HF concentration. (A) Sample **(1)**: 0.12% HF, 120 s, $\langle d \rangle = 200$ nm. (B) Sample **(2)**: 0.25% HF, 120 s, $\langle d \rangle = 200$ nm. (C) Sample **(3)**: 0.25% HF, 120 s, $\langle d \rangle = 173$ nm.

Results

Silver Substrate Fabrication. All our experiments using solution A with HF concentration varying from 0.12% to 0.75% and with various HF pretreatments show, as already noted, that silver nucleates from the region at the bottom of the well. Referring to Table 1, there are three variables, namely, HF concentration, well diameter, and time. It can be seen that low HF concentration favors pillar formation, as does small well diameter, nuclei grow with time, mainly as spherical structures, usually one nucleus is finally favored, giving rise to pillar formation. We shall still call the spheres that have grown from a nucleus, "a nucleus". Figures 3A−C show that, on going from 0.12 to 0.25% HF in $\langle d \rangle$ ~200 nm wells, the structure goes from a single nucleus in sample **(1)** to multiples in sample **(2)**, and that a smaller $\langle d \rangle$ favors a single nucleus (sample **(3)**), giving rise to pillar formation. Sample **(4)** was for small diameter,

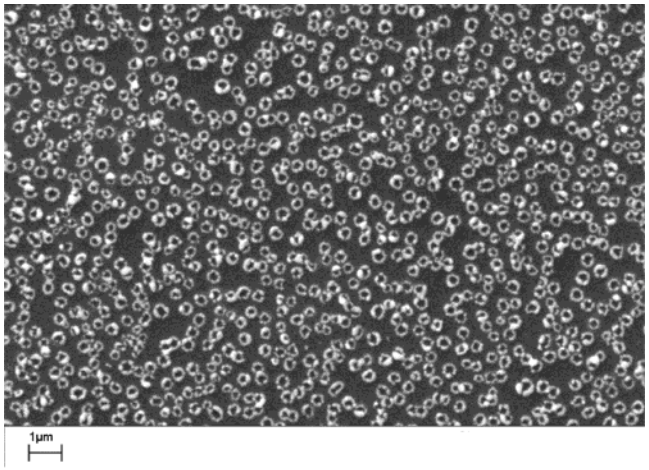

Figure 4. Effect of increase in well diameter. Silver tori on silicon after SiO_2 stripped away (5% HF for 4 min) Sample (**5**). See Table 1 for details.

increasing HF concentration (0.5% HF), and various short times. Multiple nuclei and longer time showed the emergence of the dominant nucleus that become single pillars. With 0.5% HF and larger $\langle d \rangle = 308$ nm, from 20 s to 120 s we obtain **(5)**, well defined tori, as can be seen in Figure 4. These are apparently structures that come from the joining together of sets of perhaps as many as 10−20 spherical particles, their subsequent growth favoring the shape of a torus. The well diameter is clearly a critical parameter since we have the same conditions of HF concentration and time, but with $\langle d \rangle \sim 200$ nm in sample **(6)**, giving pairs and triplets of nuclei. The effect of HF concentration as a variable is found on comparing samples **(2)**, **(6)**, and **(7)**, which is moving from pillars toward tori. Torus growth requires numerous nuclei; pillar growth comes for a smaller number where one nucleus finally dominates; continued addition of silver will finally favor pillar growth. These growth conditions are reproducible, so that, for example, pillar structures as shown in Figure 3C, or torus structures such as shown in Figure 4, may be selected for SERS study.

Silver deposition has been carried out on un-structured silicon wafers, {100} crystal plane orientation and n- and p-type, ca. 1 ohm cm. As far as carrier type goes, there is little observable difference between the silver structures obtained on these substrates. For an HF concentration of 0.25% in solution A (with 1% HF pretreatment for 1 min) the resulting silver deposit is consisted of spheres of silver averaging about 100 nm diameter plus patches of silver that have resulted from coalesced spheres, and in addition there are a low density of patches showing the bare silicon surface. When the HF concentration in solution A is 0.5% (similar pretreatment) the deposit has many more bare patches, more coalesced areas, and fewer identifiable spheres. Unfortunately the silver deposit is fairly easily detached from the silicon surface, i.e., its mechanical stability is unsatisfactory.

SERS Spectra. Figure 5 shows the pyridine Raman spectrum taken in 3 μm steps across the surface at 1 s intervals, demonstrating the uniformity of spectral output for the conditions cited. This set gave a standard deviation of ±12% for the ν_1 peak. Uniformity of this quality should be suitable for analytical work. Similar results have been obtained for random sampling over the substrate surface. For a weaker solution (5×10^{-6} M) with 17 time less adsorbed pyridine (cf. *I* vs *M*, Figure 6) the standard deviation from 31 random samplings of the surface was ±31%.

Figure 6, shows the integral peak intensity and position of the ν_1 breathing mode versus pyridine concentration. This

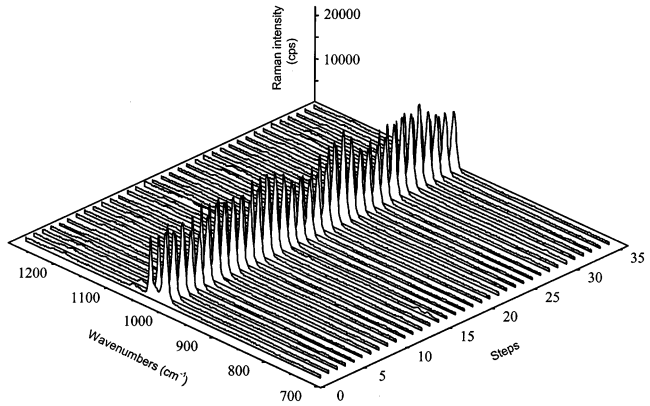

Figure 5. A set of pyridine SERS spectra taken on a tori-type structure corresponding to silver Sample (**5**), Table 1. Pyridine adsorbed from a 0.01 M pyridine in 0.1 M NaCl aqueous solution. The sample was 5 mm × 5 mm: spectra were taken along a 100 μm line in 3 μm, 1 s, steps.

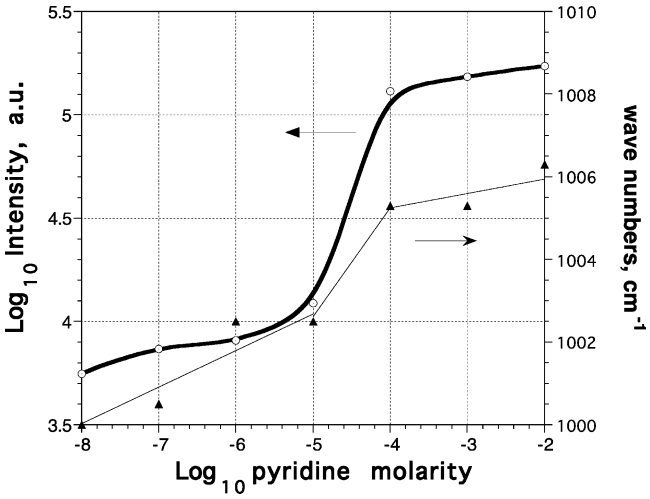

Figure 6. Adsorption of pyridine on silver: Raman intensity (ν_1 peak) and peak position versus pyridine solution concentration.

adsorption curve for pyridine on silver tori, cf. sample **(5)** (basically an adsorption isotherm), is essential, among other things, for establishing the value of the SERS enhancement. The curve shows signal saturation (assumed to be associated with monolayer coverage) starting at ca. 1×10^{-4} M concentration of pyridine: cf. Discussion section.

The variation of SERS signal for saturation coverage of pyridine on silver as a function of pretreatment of wells with HF solution, etch composition, and time, has been investigated. The intensities are self-consistent, but arbitrary, having been calibrated against the 520.6 cm^{-1} Raman line of silicon. Figure 7, taken together with the structural information in Table 1, shows the effect of HF concentration, well diameter, and deposition time, on SERS intensity. The SiO_2 delineating the wells has not been removed or reduced in size after silver deposition (see below). Set A is for dominantly pillar (cf. Figure 3) structures with more triple nuclei with increasing well size. In set B the silver structures are dominantly multi nuclei tending to tori (cf. Figure 4). Set C are mainly structures with less silver and are versions of set B with larger number of small nuclei. The largest signals are obtained from structures tending toward strings of many nuclei and tori. The least SERS activity, set A, is given by a small number of nuclei growing into a pillar.

The above spectra were obtained without removing the SiO_2, this was not deemed important since the pyridine was expected to have access to nearly all the silver. The results are sum-

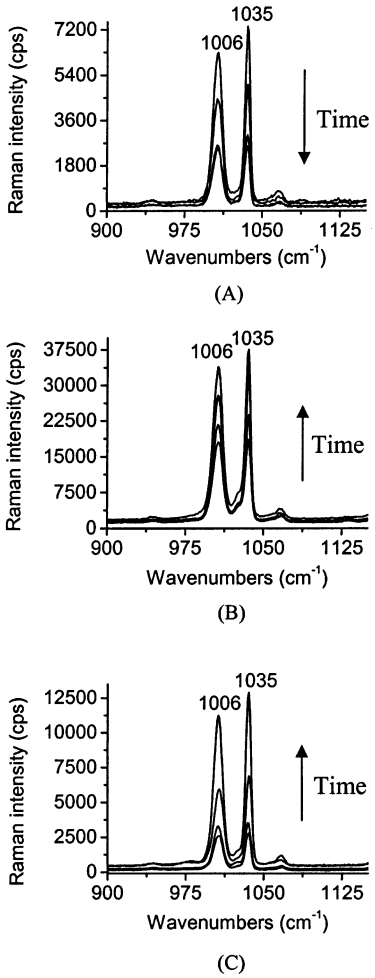

Figure 7. SERS spectra of pyridine on silver showing the effects of HF concentration, mean well diameter, and silver deposition time. Solution A was used and three sets are shown in each of which the mean diameter was increased progressively in the sequence, 173, 200, 225, to 250 nm. Set A: 0.25% HF, 120 s deposition. Set B: 0.5% HF, 120 s deposition. Set C: 0.5% HF, 30 s deposition.

TABLE 2: Pyridine/Ag SERS Spectra Enhancement Factors *G* (cf. Figure 7) for Various Structures in SiO_2 Wells

soln A, %HF: time, s	⟨*d*⟩, nm (*F*)	ν_1 peak height, cps	ν_1 peak area, cm^{-1} cps	$G \times 10^{-7}$	type of structure
		SET A			
0.25%, 120	173 (0.14)	6279	79270	0.45	pillars **(3)**
0.25%, 120	200 (0.19)	4381	56392	0.32	pillars & multi **(2)**
0.25%, 120	225 (0.24)	2601	33109	0.19	pillars & more multi
0.25%, 120	250 (0.29)	2460	31569	0.18	few pillars, many multi
		SET B			
0. 5%, 120	173 (0.14)	18090	224671	1.3	mostly triple nuclei
0. 5%, 120	200 (0.19)	21725	276569	1.6	mostly triple nuclei **(6)**
0. 5%, 120	225 (0.24)	27903	351526	2.0	multi nuclei
0. 5%, 120	250 (0.29)	33887	433560	2.5	multi nuclei & many tori
		SET C			
0. 5%, 30	173 (0.14)	2576	33321	0.19	1−3 nuclei
0. 5%, 30	200 (0.19)	3290	39472	0.23	mostly triple nuclei
0. 5%, 30	225 (0.24)	5940	73148	0.42	multi nuclei
0. 5%, 30	250 (0.29)	11248	136331	0.78	multi nuclei, some tori

TABLE 3: Effect of Oxide Removal on Relative SERS Intensity

	etch time, min				
	0	1	2	3	4
pillars & multi nuclei	1	1.07	0.93	1	0.73
mostly triple nuclei	1	1.15	0.72	0.85	0.77

marized in Table 2. The effect of oxide removal was, however, investigated, and the results are shown in Table 3. One minute of buffered HF etching (isotropic SiO_2 removal rate, ∼50 nm/min) gave a 10−15% increase in SERS intensity for samples (2) (mainly pillars), and (6) (mostly triple nuclei). Further oxide removal (2−4 min etching) gave a slight reversal of the effect. When virtually all the oxide had gone and some silver lost from the surface, there was a reduction of about 25%.

Discussion

The silver deposition studied here gave structures having a range of interrelated overall feature shapes and sizes. These substrates have excellent SERS enhancement factors for the nonresonant adsorbate pyridine, and they are stable. Also they have an overall structure that will allow the attachment of probe molecules to the non-SERS part of the substrate, while exposing the analyte to the silver with its SERS active sites.

Substrate Structure. Electroless plating is widely used in the semiconductor industry and is now a well-established technique.[14−16] The details of the silver deposition mechanism do not appear to have been elaborated. Oskam et al.[14] report that the Ag/Ag^+ couple is in contact with the semiconductor valance band and so Ag^+ discharge is a hole injection process. But we have found that the deposition rate (for our conditions) is independent of carrier type in silicon, which suggests that charge exchange may occur through electronic surface states. Since two electrochemical processes are occurring on the same electrode, the electrode potential, E_m, may be a mixed potential. The potential, E_m, will be determined by the cathodic discharge relation for Ag^+ and the anodic oxidation relation for Si, under the conditions dictated by the requirement for charge balance. The formation of nuclei and the loss of Si from the base of the wells starts from the boundary of the SiO_2/Si at the bottom of the wells (no growth starts from the floor of the wells). We do not know why this should be. One can speculate that it may be associated with a higher nucleation site density at the periphery where there is a transition from the SiO_2/Si interface to the Si/electrolyte interface. The electronic surface state density (equated to the nucleation site density) at the former interface is usually well above $10^{11} cm^{-2}$, while, according Oskam et al.,[17] the latter is about 2×10^{10} cm^{-2}. The "picture" that emerges from our observations is the following: silver nuclei grow from the boundary as spherical Ag particles, spheres coalescing with neighboring spheres as silver is added, resulting in the sort of sequence shown in Figure 8. For a fixed silver deposition time, the dimensions of the wells in the SiO_2 dictate the nature of the resulting structures, also the concentration of HF has an effect. Thus large-diameter wells will give tori when small-diameter wells for the same conditions of HF concentrated and time will give pillars. Again for fixed time and well diameter, high HF concentration favors tori while lower concentrations favor pillars. What is apparent is that all growth starts from nucleated spheres growing out from around the periphery. First, there is what we loosely call a torus, which we will observe if the well diameter is large enough. The torus on growing further coalesces with other spheres as it grows, making small numbers

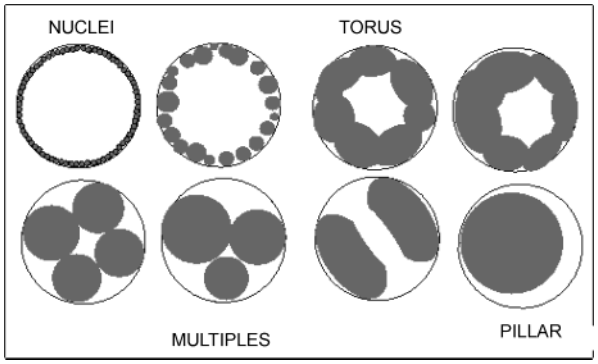

Figure 8. Depiction of stages in the growth of silver spheres at the bottom of the well at the Si/SiO_2 boundary.

of spheres. Finally, one sphere dominates and fills much of the well and grows out as a pillar; this if allowed to grow further develops a head. It is visually apparent for most of the structures seen that the overall figure is made from smaller intersecting structures with convex surfaces. It is probably the regions of intersection of these smaller "spheres" that are particularly SERS active.

Enhancement Factor. The overall enhancement of the Raman signal is of great importance, and knowledge of its magnitude is obviously of central concern. Following the procedure of Tian and his group,[18] the SERS enhancement factor, *G*, is defined as

$$G = (I_{Ag}/N_{ads})/(I_{sol}/N_{sol}) \quad (1)$$

where I_{Ag} is the integral intensity (**total peak area**) of the Raman signal obtained from N_{ads} adsorbed pyridine molecules, and I_{sol} is the corresponding intensity from the N_{sol} pyridine molecules in the excitation volume of the Gaussian beam. The value of N_{ads} for **monolayer coverage** is obtained from the following relation:

$$N_{ads} = RgSA/\sigma \quad (2)$$

where *R* is a surface roughness factor, *g* is the estimated geometrical (smooth) area of the silver adsorbent per unit area, *S* is the fraction of silver area "seen" by the laser beam, *A* is the area of the focal spot of the laser, and σ is the area occupied by a molecule of adsorbent at monolayer coverage. On considering the solution, in principle, all the pyridine molecules within the illuminated volume of solution contribute to N_{sol}. But, the collection efficiency for the light scattered from the pyridine molecules in each plane of the solution varies with confocal depth. However, one can define an effective layer depth, *h*, within which each pyridine molecule yields the same contribution to the Raman signal as those localized in the ideally focused plane. In this case, N_{sol} is given by

$$N_{sol} = Ahn_{sol} \quad (3)$$

where n_{sol} is the number of molecules per unit volume of solution. Combining these relations, the expression for G is as follows:

$$G = I_{Ag}\sigma hn_{sol}/I_{sol}RgS \quad (4)$$

As an example we consider the results shown in Figure 4, where we need to know how many molecules of pyridine there are in the spot area with the torus structure of sample **(5)**.

g: Estimated by taking the outer diameter, d_o, of the torus equal $\langle d \rangle$ nm, the inner diameter, d_i, equal ($\langle d \rangle$ -138 nm), given the array characteristics $\langle d \rangle = 310$ nm and $F = 0.36$. The ratio of the surface area of torus to the surface area of the disk of the outer torus (bottom of the well) is $(\pi^2/4)[(d_o - d_i)(d_o + d_i)]/(\pi/4)d_o^2 = 2.2$, when $d_o = 310$ nm and $d_i = 170$ nm. With $F = 0.36$, the ratio of the area of silver to the area of planar substrate *g* is $0.36 \times 2.2 = 0.79$.

R: Inspection of the electron micrograph shows some undulations of the torus structure, so it will be assumed (conveniently!) that the above ratio can be increased by 25% (i.e., $R = 1.25$) so $Rg = 1$.

S: Shadowing effect such that at least half the pyridine molecules will not "see" the exciting laser beam; $S = 0.5$

h: It was found experimentally that $h = 135$ μm (1.35×10^{-4} m).

σ: This parameter is estimated[18] to be 0.3 nm^2 (3×10^{-19} m^2).

n_{sol}: The concentration of pyridine in water is usually expressed as a molarity (*M*), and multiplication of *M* by 6.023×10^{26} converts this to n_{sol} molecules m^{-3}. With these quantities we obtain the following:

$$G = 4.88 \times 10^4 \times M \times I_{Ag}/I_{sol} \quad (5)$$

The intensities are the integrated intensities of the peak centered about 1006 cm^{-1} (see discussion below).

In the case of adsorption from a 10^{-2} M solution of pyridine onto sample **(5)** (tori), we obtain monolayer coverage and find

$$I_{Ag}\text{: } 258473 \text{ counts cm}^{-1}\text{/s}$$

$$I_{sol}\text{: } 73.7 \text{ counts cm}^{-1}\text{/s (300 s sample time)}$$

for a $M = 10^{-1}$ molar solution of pyridine.

With these values, eq 5 gives $G = 1.7 \times 10^7$. Modifications of this structure have given *G* about equal to about 10^8. With this procedure it is possible to make a quantitative comparison of various substrates, the greatest difficulty being that of obtaining a reliable estimate of the product of the three constants, *Srg*, especially the roughness, *g*. This latter uncertainty probably results in an upper limit error of about $\pm 50\%$ in estimating *G*.

Adsorption Isotherm and SERS Activity. A major question for the application of SERS is the relation between the intensity of the SERS signal and the amount of adsorbed analyte. SERS is taken by a number of workers to derive from singularities in the substrate structure (edges, wedges, sharp tips, etc.) producing strong electromagnetic field localization interacting with locally adsorbed molecules.[19] It is possible, but by no means a universal truth, that SERS intensity and adsorbate surface binding energy are simply linked together. We can consider Figure 6, showing the SERS intensity versus pyridine solution concentration. And at this point it is appropriate to introduce eq 6, the expression for the standard free energy, $\Delta\mu^\circ$, of pyridine adsorption onto silver from an aqueous solution of molar concentration, *x*:

$$-\Delta\mu^\circ = RT \ln[(\Theta/1 - \Theta)/x] \quad (6)$$

where Θ is the surface fractional coverage, and *RT* has its usual meaning. The standard states are $\Theta = 1/2$ and $x = 1$, and the conditions of the Langmuir adsorption isotherm are taken to apply. The jump in the *I* versus *x* curve between $x = 10^{-5}$ and 10^{-4} M is taken to represent a corresponding Θ from near 0 to near 1 over the greater part of the silver surface. In this case $\Theta = 1/2$ at $x = 6.5 \times 10^{-5}$ M, so that from eq 6, $-\Delta\mu^\circ = 9.64RT$ (24 kJ mol^{-1} at 300 K). We have inferred that $\Theta \propto I$, and ask the question what adsorbate properties would give this result?

Clearly if all sites, SERS and non-SERS, had the same adsorption energy (consistent with the Langmuir isotherm) we would obtain the above result. Alternatively, consider the case that there is a small fractional surface density of SERS active sites with large standard free energy of adsorption, the rest of the surface having a lower energy. In that case, the jump would represent only a small amount of pyridine adsorption: it might, therefore, be the upper region, 10^{-4} M to 10^{-2} M, that is the range of pyridine monolayer formation! However, the free energy of adsorption of pyridine from aqueous solution onto silver (polished) has been measured by Chen et al.[20] and found to be in the range -20.1 to -21.8 kJ mol^{-1}, in good agreement with our finding of -24 kJ mol^{-1}. Further support for the interpretation of the *I* versus concentration curve comes from considering the vibrational data in Figure 6. There a jump is shown in wavenumber over the same solution concentration range, 10^{-5} M to 10^{-4} M, as the jump in *I*. This is interpreted as arising from a configurational change in the adsorbed pyridine as it goes through the process of monolayer formation. The observed shift in wavenumber of the Raman peak is consistent with the calculations of Wu et al.[21] for the pyridine−Ag system. The evidence therefore points to the original supposition that SERS intensity, *I*, could, for pyridine/silver, be proportional to total Θ. Adsorption isotherms such as ours have been obtained for a similar range of molecules.[22,23] This linear relation between *I* and Θ suggests that the "SERS sites" are not correlated with the **strong** adsorption sites of atomistic dimensions, but are large, covering areas sufficiently large to be typical of an average coverage, thereby smearing out effects of adsorption heterogeneity. We have already proposed above that SERS sites arise in the regions of intersecting spheres. Target (analyte) molecules that are very different from pyridine, e.g., rhodamine 6G may well respond differently and behave as though (large) SERS regions and adsorption sites are to some extent correlated: this will then present a difficulty for quantitative analysis that must be overcome.

The variation in *G* listed in Table 2 is small considering the range of structures. But this may be explained by the fact that the structures are built up from coalesced spheres giving rise to a range of super-structures. Further experiments are needed to separate the significance of inter-well contacts from intra-well contacts as far as SERS enhancement goes. The margin of evidence points to inter-well effects giving greater *G*: but it is a small margin of evidence.

We have established that the substrates prepared here are uniform as to SERS activity when saturated in pyridine ($x = 10^{-2}$ M), i.e., when every available site has adsorbate (cf. Figure 6). But it is also important to know what the uniformity is when the coverage is low. We find that for $x = 5 \times 10^{-6}$ M there is uniformity in *I* (within $\pm$31%) and that the signal comes from ca. 0.077 of a monolayer.

Conclusions

Mechanically stable silver structures, produced by a galvanic exchange process on silicon wafers, can be made giving useful SERS substrates with a uniform (large) enhancement factor for pyridine over a large area (many square mm). The SERS signal would appear to sample an area of the adsorbent large compared with a pyridine molecule, resulting in the SERS signal being proportional to the adsorbate coverage. In other words, the SERS signal is not proportional to a particular surface density of sites (singularities) of roughly atomic dimensions. With this realization, we have been able to obtain an adsorption isotherm for pyridine on silver. This, in turn, allowed us to obtain the intensity per adsorbate molecule, together with other things, needed for estimating the SERS enhancement factor. We now have highly active structured silver substrates that are spatially uniform in SERS signal for small adsorbed molecules and yield useful adsorption isotherms. We are now in a better position to investigate the SERS properties of these silver structures in the single molecule regime and at different wavelengths for oligonucleotides. This work has addressed the analytical problem and not the mechanistic aspects of SERS, and the overall enhancement that we measure does not distinguish between various processes.

Acknowledgment. We thank EPSRC for supporting this project. We thank Renishaw plc. for help in the up-grade of the Raman microscope.

References and Notes

(1) Moskovits, M. *Rev. Mod. Phys*. **1985**, *57*, 783.
(2) Chang, R. K. *Ber. Bunsen-Ges. Phys. Chem*. **1987**, *91*, 296.
(3) Otto, A.; Mrozek, I.; Grabhorn, H.; Akemann, W. *J. Phys.: Condens. Matter* **1992**, *4*, 1143.
(4) Tian, Z. Q.; Ren, B.; Wu, D. Y. *J. Phys. Chem*. **2002**, *106*, 9463.
(5) Fleischman, M.; Hendra, P. J.; Mcquillan, A. J. J. *J. Chem. Soc., Chem. Commun*. **1973**, 80.
(6) Liao, L. P.; Bergman, J. G.; Chemla, J. G.; Wokaun, A.; Melngailis, J.; Hawryluk, A. M.; Economou, A. M. *Chem. Phys. Lett*. **1991**, *82*, 355.
(7) Nie, S. M.; Emory, S. R. *Science* **1997**, *275*, 1102.
(8) Gunnersson, I.; Petronis, S.; Kasemo, B.; Xu, H.; Bjerneld, L.; Kall, M. *NanoStructured Mater*. **1999**, *12*, 783.
(9) Green, M.; Garcia-Parajo, M.; Khaleque, F.; Murray, R. *Appl. Phys. Lett*. **1993**, *66*, 264.
(10) Green, M.; Tsuchiya, S. *J. Vac. Sci. Technol., B* **1999**, *17*, 2074.
(11) Tsuchiya, S.; Green, M.; Syms, R. R. A. *Electrochem. Solid State Lett.* **2000**, *3*, 44.
(12) ten Kortenaar, M. V.; de Goeij, J. J. M.; Kolar, Z. I.; Frens, G.; Lusse, P. J.; Zuiddam, M. R.; van der Drift, E. *J. Electrochem. Soc*. **2001**, *148*, C28.
(13) Green, Mino. Unpublished work.
(14) Oskam, G.; Long, J. G.; Natarajan A.; Searson, P. C. *J. Phys. D: Appl. Phys.* **1998**, *31*, 1927.
(15) *Electroless Plating: Fundamentals and Applications*; Mallory, G. O., Hajdu, J. B., Eds.; American Electroplaters and Surface Finishers Society, 1990.
(16) Leske, M.; Schultz, J. W.; Thonissen, M.; Munder, H. *Thin Solid Films* **1995**, *255*, 63.
(17) Oskam, G.; Hoffmann, P. M.; Searson, P. C. *Phys. Rev. Lett*. **1996**, *76*, 1521.
(18) Cai, W. B.; Ren, B.; Li, X. Q.; She, C. X.; Liu, F. M.; Cai, X. W.; Tian, Z. Q. *Surf. Sci*. **1998**, *406*, 9.
(19) Moskovits, M.; Tay, L. L.; Yang, J.; Haslett, T. *Top. Appl. Phys.* **2002**, *82*, 215.
(20) Chen, C. K.; Heinz, T. F.; Ricard, D.; Shen, T. R. *Chem. Phys. Lett*. **1981**, *83*, 455.
(21) Wu, D. Y.; Ren, B.; Jiang, Y. X.; Xu, X.; Tian, Z. Q. *J. Phys. Chem. A* **2002**, *106*, 9042.
(22) Vo-Dihn, T.; Hiromoto, M. Y. K.; Begun, G. M.; Moody, R. L. *Anal. Chem*. **1985**, *56*, 1667.
(23) Pal, T.; Narayanan, V. A.; Stokes, D. L.; Vo-Dihn, T. *Anal. Chem. Acta* **1998**, *368*, 21.